Characterization of a thicknessshear mode quartz resonator with multiple nonpiezoelectric layers

Victoria Edwards Granstaff and Stephen J. Martin

Citation: Journal of Applied Physics **75**, 1319 (1994); doi: 10.1063/1.356410
View online: http://dx.doi.org/10.1063/1.356410
View Table of Contents: http://scitation.aip.org/content/aip/journal/jap/75/3?ver=pdfcov
Published by the AIP Publishing

Characterization of a thickness-shear mode quartz resonator with multiple nonpiezoelectric layers

Victoria Edwards Granstaff and Stephen J. Martin
Sandia National Laboratories, Albuquerque, New Mexico 87185

(Received 22 July 1993; accepted for publication 21 October 1993)

This paper describes a one-dimensional analysis of a piezoelectric resonator with multiple nonpiezoelectric layers of arbitrary thickness and complex shear modulus. This analysis shows under what conditions the simple Butterworth–Van Dyke (BVD) lumped-element equivalent circuit can be used to extract the properties of these layers, and provides a theoretical basis for doing so under these conditions. The method presented here is based on the physics of wave propagation, but uses transmission line techniques to transform the equations and boundary conditions into a simple string of 2×2 matrix multiplications, which easily accommodate any number of layers. An analysis of the AT-cut quartz/polymer/liquid composite resonator is presented in detail because of its importance in sensor and electrochemical quartz crystal microbalance applications. The analysis shows that adding the polymer and liquid impedances in the motional arm of a BVD circuit is *not* valid near the polymer film resonance, but is appropriate for a thin, rigid polymer film in contact with a liquid.

I. INTRODUCTION

Quartz resonators, such as quartz crystal microbalances (QCMs), are commonly used to measure mass deposition rates in vacuum. These devices operate by applying an oscillating electric field across the thickness of a piezoelectric AT-cut quartz disk that induces a shear-thickness mode of mechanical oscillation. At resonance, a standing wave is created and the amplitude of the quartz oscillation is maximized. Figure 1 illustrates the shear displacement profiles of quartz for the fundamental and third-harmonic modes of oscillation. At the series resonant frequency, the electrical admittance magnitude (inverse of impedance) is maximum; at the parallel resonant frequency, the admittance magnitude is minimum.

The simplest use of these devices is to measure the decrease in resonant frequency induced by mass deposition on the surface of a quartz disk. For small mass loadings (causing up to a 2% decrease in resonant frequency),[1] the frequency decrease is proportional to the mass per unit active area.[2] The "Z-match" technique[3] and the two-frequency Z-determination method[1] extend the usable frequency range for lossless deposited films. Although Benes[1] presents a resonance equation for a quartz resonator with a single lossy layer, the *detailed* analysis in the paper is not valid for lossy layers, such as rubbery polymer or liquid layers.

Recently, quartz resonators have become popular for use in liquids. Applications include sensors based on mass or liquid property changes,[4–6] and electrochemical quartz crystal microbalances (EQCMs).[7,8] EQCMs are also used to study electrodeposition,[9–11] corrosion,[12,13] batteries,[14–16] and electroactive polymers.[7,8,17] Many of these applications use a quartz resonator having multiple layers, including a contacting fluid. Although we have previously presented a convenient analysis technique for the quartz/rigid-mass/liquid system,[4] there is a need to understand the behavior of a quartz resonator having a nonrigid coating, such as a polymer, in contact with a liquid. When polymer losses and polymer–liquid interactions are significant, existing mass measurement techniques are inaccurate.

Presented here is a one-dimensional analysis that applies to a piezoelectric resonator with multiple nonpiezoelectric planar layers. There are no restrictions on the layer thicknesses or complex shear moduli. Although other investigators have demonstrated that mass sensitivity varies with radial position,[18,19] electrical admittance data represent an average over the active area, and one-dimensional models have been used successfully to fit experimental data.[1–4,20–22] These one-dimensional models work especially well if the device parameters are first extracted from measurements made on the unperturbed device.[4]

Although transmission line techniques[23,24] are convenient for modeling one-dimensional, multilayer structures, most of the previous modeling of quartz resonators has not taken full advantage of these methods. This paper presents a technique that is easy to implement numerically, and applies to a quartz resonator having any number of layers of arbitrary thickness and complex shear modulus. We also discuss the range of applicability of simpler modeling methods. Readers less interested in the mathematical details may wish to skip the theory section.

Previous models have used either of two methods. The first method is to model the composite resonator as an electrical equivalent circuit, known as a Butterworth–Van Dyke (BVD) circuit,[25] as shown in Fig. 2. The element denoted Z_e in the motional arm of the circuit is proportional to the acoustical (mechanical) impedance, Z_s, at the sensing surface of the quartz resonator. This technique, described by Martin, Granstaff, and Frye,[4] Martin and Frye,[20] and Martin *et al.*[26] is very useful when the magnitude of the surface mechanical impedance is much smaller than the quartz characteristic impedance, Z_q. Thin, rigid films and low-viscosity liquids satisfy this criterion.

Another method for modeling composite resonators is to solve the wave equations and the piezoelectric constitu-

 0021-8979/94/75(3)/1319/11/$6.00

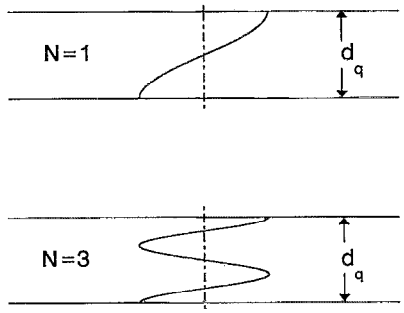

FIG. 1. Side cross-sectional view of AT-cut quartz wafer, showing shear displacement profiles for the fundamental and third-harmonic resonances.

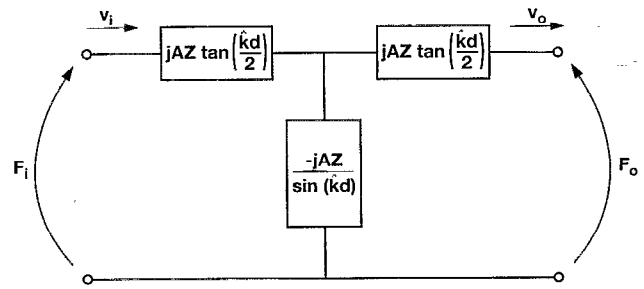

FIG. 3. Two-port Mason model of nonpiezoelectric layer (adapted from Rosenbaum, see Ref. 25).

tive equations, subject to the appropriate boundary conditions at each interface. This set of differential equations and boundary conditions reduces to a set of algebraic equations to be solved for the boundary-condition integration constants.[27] Although only one of these constants is necessary to describe the electrical admittance vs frequency, the algebra required to obtain it is quite cumbersome and is not readily extendible to more layers.

The method used here is based on a Mason model as described in Rosenbaum.[25] The Mason model is a transmission line representation of the physically based one-dimensional equations and boundary conditions, and it does not use any approximations other than the one-dimensional assumption. The Mason model represents each nonpiezoelectric layer by a 2×2 matrix, so that additional layers are included by cascading matrices. Similar methods have also been used for calculating the optical characteristics of multilayer materials.[28] Although manipulating long products of these matrices by hand can be tedious, the matrix multiplication is easily programmed on a computer. In addition, these methods demonstrate a theoretical basis for the BVD equivalent-circuit method and the conditions under which it applies. Thus, one can determine whether the convenient BVD equivalent-circuit model is valid, and, if not, apply a simple method for analyzing multiple layers with arbitrary thicknesses and complex shear moduli.

II. THEORY

Following Rosenbaum,[25] we use a two-port Mason equivalent circuit (shown in Fig. 3) to represent a linear model of an arbitrary nonpiezoelectric layer. Note Fig. 3 differs from Fig. 6.9 in Rosenbaum[25] because the characteristic impedance Z should not include the surface area A. Although this representation is written for a layer of finite thickness, it can also represent an infinitesimally thin or an infinitely thick layer, by taking the appropriate limits of the layer thickness. In Figs. 3–6, the acoustical variables are analogous to electrical variables: force or stress (force per unit area) corresponds to voltage, particle velocity corresponds to current, and mechanical impedance (ratio of stress to particle velocity) is analogous to electrical impedance. A Mason model can also represent a piezoelectric layer, but the circuit has two acoustical ports and one electrical port (see Fig. 4). Figure 4 is a representation of the

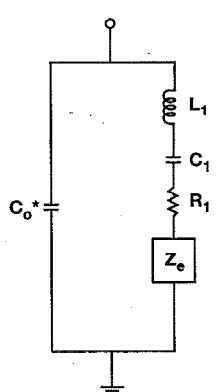

FIG. 2. Butterworth–Van Dyke equivalent circuit model of coated quartz, showing element Z_e contributed by film(s) on the quartz. C_0^* is the quartz static capacitance, accounting for parasitic capacitance.

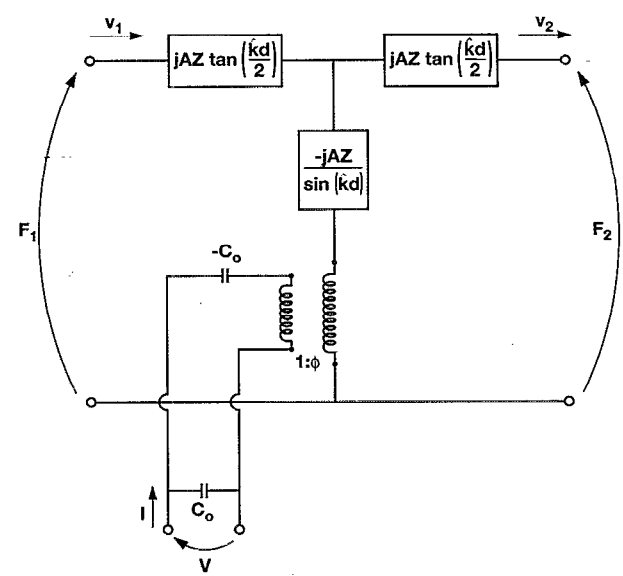

FIG. 4. Three-port Mason model of piezoelectric quartz (adapted from Rosenbaum, see Ref. 25).

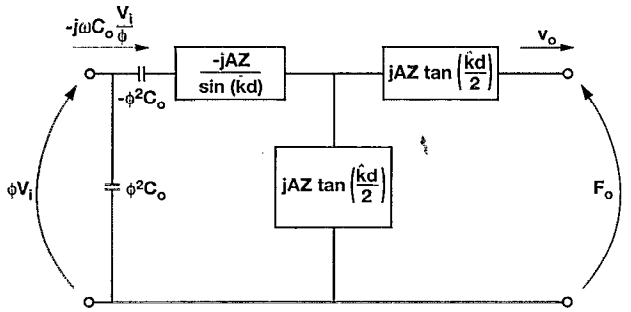

FIG. 5. Two-port Mason model of piezoelectric quartz with one stress-free interface (adapted from Rosenbaum, see Ref. 25).

governing force-balance equations for the piezoelectric layer. The transformer describes the conversion between the electrical and acoustical variables, where the acoustical voltage is defined as the force. Benes uses a three-port model to describe quartz resonators;[1] however, in this work, we simplify the three-port model to a two-port model by connecting an appropriate impedance across the acoustical port representing the side of the quartz having the uncoated electrode. The convention in this paper is that the coated sensing electrode is on the "top" side of the quartz. If the bottom electrode has a significant areal mass density, its impedance is $j\omega\rho_s$, where ρ_s is the areal mass density of the electrode (kg/m^2). For simplicity, however, we make the commonly accepted assumption that the bottom electrode is thin enough to model its impedance as a short (zero impedance), corresponding to a stress-free interface. The transformer in Fig. 4 is then eliminated by standard circuit methods[29] to yield the two-port equivalent-circuit model of the quartz with one stress-free interface, as shown in Fig. 5. This circuit model has one acoustical port and one electrical port.

A simple implementation of the two-port Mason model, as detailed in Rosenbaum,[25] is to write a matrix equation to express the output current and voltage as a linear function of the input current and voltage and the acoustic parameters of the layer, i.e.,

$$\begin{bmatrix} V_o \\ I_o \end{bmatrix} = \begin{bmatrix} A' & B' \\ C' & D' \end{bmatrix} \begin{bmatrix} V_i \\ I_i \end{bmatrix}, \tag{1}$$

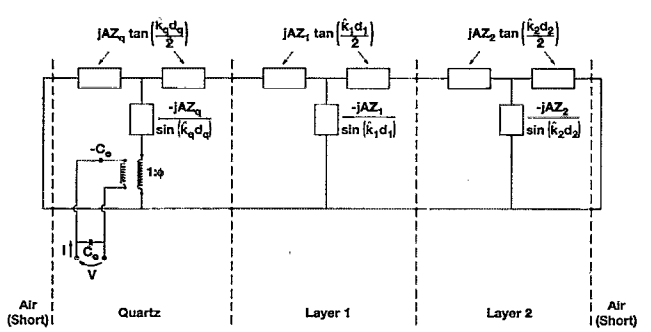

FIG. 6. Mason model of composite resonator having a stress-free interface on one side, and two arbitrary films on the other side (adapted from Rosenbaum, see Ref. 25).

where the voltages V and the currents I may be either electrical or acoustical variables. Note that if the output variables are known, the input variables are calculated by multiplying both sides of Eq. (1) by the inverse of the $A'B'C'D'$ transformation matrix. Because the matrices derived in Rosenbaum take the quartz electrical port to be the input, we use the inverses of the matrices given in Rosenbaum to calculate the impedance at the electrical port

$$\begin{bmatrix} V_i \\ I_i \end{bmatrix} = \begin{bmatrix} A & B \\ C & D \end{bmatrix} \begin{bmatrix} V_o \\ I_o \end{bmatrix}. \tag{2}$$

In addition, we define the acoustical voltage to be stress (for consistency with the definition of the impedance as the ratio of stress to particle velocity). At the stress-free top interface of the composite device, the acoustical voltage V_o is zero, while I_o is unknown. The impedance calculations, however, do not depend on I_o, because, with the linear model of the solid, it cancels out of the numerator and denominator. The transformation matrix entries in Eq. (2), for a nonpiezoelectric layer, are as follows:[25]

$$A=\cos(\hat{k}d), \tag{3a}$$

$$B=jZ\sin(\hat{k}d), \tag{3b}$$

$$C=j\frac{\sin(\hat{k}d)}{Z}, \tag{3c}$$

$$D=\cos(\hat{k}d), \tag{3d}$$

where $\hat{k}$ and d are the complex propagation constant and the layer thickness, respectively. Z is the characteristic impedance of the layer material,

$$Z=\sqrt{\rho G}, \tag{4}$$

where G is the complex shear modulus and ρ is the mass density. The complex propagation constant, $\hat{k}$, is defined such that

$$\gamma=j\hat{k}=j\omega\sqrt{\rho/G}, \tag{5}$$

where γ is the wave propagation constant and ω is the angular frequency of oscillation.

For a piezoelectric layer, the matrix entries relating the electrical voltage and current to the acoustical voltage (stress) and current (particle velocity) are as follows:

$$A_q=\left[\frac{j\phi^2}{\omega C_0}+\mathbf{A}(a+b)\right]\Big/\phi a, \tag{6a}$$

$$B_q=\left(\frac{2j\phi^2 a}{\omega C_0}+\mathbf{A}(a^2+2ab)\right)\Big/\phi a, \tag{6b}$$

$$C_q=\frac{j\omega C_0\mathbf{A}(a+b)}{\phi a}, \tag{6c}$$

$$D_q=\frac{j\omega C_0\mathbf{A}(a^2+2ab)}{\phi a}, \tag{6d}$$

where

$$a=jZ_q\tan\left(\frac{\hat{k}_q d_q}{2}\right), \tag{7a}$$

and

$$b=\frac{-jZ_q}{\sin(\hat{k}_q d_q)}. \tag{7b}$$

$\hat{k}_q$ is the complex wave propagation constant for quartz, and d_q is the quartz thickness. C_0, the capacitance of the AT-cut quartz, is

$$C_0=\frac{\epsilon_{22}\mathbf{A}}{d_q}, \tag{8}$$

where ϵ_{22} is the quartz permittivity, and $\mathbf{A}$ is the active electrode area. Z_q, the characteristic impedance of the quartz, is analogous to Eq. (4):

$$Z_q=\sqrt{\rho_q \bar{c}_{66}}, \tag{9}$$

where $\bar{c}_{66}$ is the piezoelectrically stiffened complex shear modulus of the lossy quartz. Note that in contrast to the expressions given in Rosenbaum,[25] the electrode area must appear in Eqs. (6a)–(6d) to be consistent with the definition of the quartz characteristic impedance, Z_q [see Eq. (9)]. The turns ratio, ϕ, of the transformer in Fig. 4, is

$$\phi=hC_0=(e_{26}/\epsilon_{22})C_0, \tag{10}$$

where e_{26} is the piezoelectric stress constant. Recall that these transformation matrices are used to calculate the electrical quantities from known acoustical quantities.

For fitting data, it is convenient to reduce the number of adjustable parameters. From Eq. (2),

$$V_n=A_nV_{n+1}+B_nI_{n+1}, \tag{11a}$$

and

$$I_n=C_nV_{n+1}+D_nI_{n+1}, \tag{11b}$$

where the layer index, n, starts at zero for the quartz and ends with N for the top layer. Therefore,

$$Z_n=\frac{V_n}{I_n}=\frac{A_nZ_{n+1}+B_n}{C_nZ_{n+1}+D_n}. \tag{12}$$

Defining

$$Q_n=\frac{B_nC_n}{A_nD_n}=-\tan^2(\hat{k}_n d_n)=\tanh^2(\gamma_n d_n); \tag{13}$$

Eq. (12) is rewritten as

$$Z_n=\left[\frac{A_n}{C_n}\left(\frac{C_n}{D_n}Z_{n+1}+Q_n\right)\right]\Big/\left(\frac{C_n}{D_n}Z_{n+1}+1\right). \tag{14}$$

Since

$$\frac{A_n}{C_n}=\frac{Z_n}{\tanh(\gamma_n d_n)}=\frac{1}{C_n/D_n} \tag{15}$$

for a nonpiezoelectric layer, the evaluation of Eq. (14) requires only the two complex parameters A_n/C_n and Q_n. The calculations begin by setting $Z_{N+1}=0$ (zero stress at the top of the composite resonator), where N is the number of layers on the sensing side of the quartz; the remaining Z_n's are calculated recursively.

Note that, in agreement with electrical engineering textbooks,[23] if a load impedance, Z_L, is imposed at the output port, so that $Z_L=V_0/I_0$, the resulting input impedance is, from Eqs. (11a) and (11b),

$$Z_i=\frac{V_i}{I_i}=\frac{V_0\cos(\hat{k}d)+I_0jZ\sin(\hat{k}d)}{V_0j[\sin(\hat{k}d)/Z]+I_0\cos(\hat{k}d)}$$

$$=Z\left(\frac{Z_L\cosh(\gamma d)+Z\sinh(\gamma d)}{Z\cosh(\gamma d)+Z_L\sinh(\gamma d)}\right), \tag{16}$$

where Z is the characteristic impedance of the layer. If the top of the layer is stress free ($Z_L=0$), the impedance at the bottom of the layer is $Z\tanh(\gamma d)$.

The procedure for modeling a quartz resonator with multiple layers is to stack the layers (represented by concatenating the 2×2 matrices for each layer), starting with the knowledge that the top of the composite resonator is stress free, and working toward calculating the variables at the electrical port. Figure 6 is an example of a Mason model of a composite system having two nonpiezoelectric layers on a quartz resonator. Applying the matrix multiplication principle embodied in Eqs. (2) and (11) to the example in Fig. 6 gives

$$\begin{bmatrix}V\\I\end{bmatrix}=\begin{bmatrix}A_q & B_q\\C_q & D_q\end{bmatrix}\begin{bmatrix}A_1 & B_1\\C_1 & D_1\end{bmatrix}\begin{bmatrix}A_2 & B_2\\C_2 & D_2\end{bmatrix}\begin{bmatrix}V_2\\I_2\end{bmatrix}$$

$$=\begin{bmatrix}A_q(A_1B_2I_2+B_1D_2I_2)+B_q(C_1B_2I_2+D_1D_2I_2)\\C_q(A_1B_2I_2+B_1D_2I_2)+D_q(C_1B_2I_2+D_1D_2I_2)\end{bmatrix} \tag{17}$$

with $V_2=0$ for the stress-free interface on top of layer 2. The impedance at the electrical port can then be calculated from V/I, noting that the unknown I_2 cancels out. The impedance is, therefore,

$$Z=\frac{A_qV_q+B_qI_q}{C_qV_q+D_qI_q}, \tag{18}$$

where, for two layers,

$$V_q=A_1B_2+B_1D_2=jZ_1\left[\left(\frac{Z_2}{Z_1}\right)\cos(\hat{k}_1d_1)\sin(\hat{k}_2d_2)\right.$$

$$\left.+\sin(\hat{k}_1d_1)\cos(\hat{k}_2d_2)\right] \tag{19}$$

and

$$I_q=C_1B_2+D_1D_2$$

$$=-\left(\frac{Z_2}{Z_1}\right)\sin(\hat{k}_1d_1)\sin(\hat{k}_2d_2)+\cos(\hat{k}_1d_1)\cos(\hat{k}_2d_2). \tag{20}$$

Note that, for any number of layers, V_q/I_q is the acoustic impedance, Z_s, seen at the quartz surface because V_q/I_q is the impedance calculated by multiplying the transformation matrices for the nonpiezoelectric layers only.

It will be shown that, under certain conditions, it is valid to use an element proportional to this surface impedance, Z_s, in the motional arm of a BVD equivalent circuit. To convert Eq. (18) into a BVD circuit representation, the electrical admittance is rewritten as

$$Y=\frac{C_qV_q+D_qI_q}{A_qV_q+B_qI_q}=\frac{C_qZ_s+D_q}{A_qZ_s+B_q}=j\omega C_0\left(1+\frac{Y_m}{j\omega C_0}\right), \quad (21)$$

where Y_m is the admittance of the motional arm of the circuit (see Fig. 2). From this expression, the impedance of the motional arm can be calculated as

$$Z_m=\frac{A_qZ_s+B_q}{D_q-j\omega C_0B_q+Z_s(C_q-j\omega C_0A_q)}. \quad (22)$$

Although this expression is complicated, it simplifies when Z_s is small, such that the motional impedance is proportional to the surface mechanical impedance.

When using the present model to calculate admittance versus frequency data over a large frequency range, the frequency mesh size should be allowed to vary according to how fast the admittance values are changing relative to the admittance maximum that occurs at resonance. This will prevent the calculation from overlooking a sharp resonance without creating unmanageably large data files. Because the resonances must be found numerically, for arbitrary layers, the criterion for choosing the mesh size must reflect the desired relative precision in the calculated admittance versus frequency data. When fitting experimental data, the mesh spacing would match that used in the experiment, and, after fitting data for the uncoated resonator, the two complex parameters, A_n/C_n and Q_n, would be fit using a nonlinear optimization technique. This fitting is easier if the properties of the quartz and each film are determined individually, either by using separate crystals or by measuring the properties before and after coating a single crystal.

III. LIMITING CASES

A. Unloaded quartz ($Z_s=0$)

For unloaded quartz, $Z_s=0$ because the top quartz interface is stress free. Substituting into Eq. (22), and using B_q and D_q from Eqs. (6b) and (6d) gives the motional impedance,

$$Z_m=\frac{j}{\omega C_0}+\frac{\mathbf{A}(a+2b)}{2\phi^2}. \quad (23)$$

Equations (7)–(10) and trigonometric identities[30] are used with the following resonance conditions and definitions:[4]

$$\tan\left(\frac{\hat{k}_qd_q}{2}\right)=\frac{4\hat{k}_qd_q}{(N\pi)^2-(\hat{k}_qd_q)^2}, \quad (24)$$

$$K^2=\frac{K_0^2}{1+j\xi}, \quad (25a)$$

$$K_0^2=\frac{e_{26}^2}{\bar{c}_{66}\epsilon_{22}}, \quad (25b)$$

$$\hat{k}_qd_q=\omega d\sqrt{\rho_q/\bar{c}_{66}}=\hat{k}_0d_q/\sqrt{1+j\xi}, \quad (25c)$$

$$\xi=\frac{\omega\eta_q}{\bar{c}_{66}} \quad (25d)$$

to give

$$Z_m=j\frac{(N\pi)^2}{8\omega C_0K_0^2}-j\frac{(N\pi)^2}{8\omega C_0K_0^2}+\frac{(N\pi)^2\eta_q}{8C_0K_0^2\bar{c}_{66}}$$

$$=j\omega L_1+\frac{1}{j\omega C_1}+R_1, \quad (26)$$

where N is the harmonic number, K_0^2 is the electromechanical coupling factor, and the circuit elements L_1, C_1, and R_1 are

$$C_1=\frac{8K_0^2C_0}{(N\pi)^2}, \quad (27a)$$

$$L_1=\frac{1}{\omega_s^2C_1}, \quad (27b)$$

$$R_1=\frac{\eta_q}{\bar{c}_{66}C_1}. \quad (27c)$$

These expressions, which describe bare quartz as a BVD equivalent circuit model, are in agreement with Martin, Granstaff, and Frye[4] at resonance.

B. Small $|Z_s/[Z_q\tanh(\gamma_qd_q/2)]|$

If $|Z_s/[Z_q\tanh(\gamma_qd_q/2)]|$ is small (low surface impedance), the small-x approximation $1/(1+x)\cong 1-x$ can be used to approximate Eq. (22) as

$$Z_m\cong\frac{B_q}{D_q-B_q\,j\omega C_0}+Z_s\left(\frac{A_q}{D_q-B_q\,j\omega C_0}\right.$$

$$\left.-\frac{B_q(C_q-j\omega C_0A_q)}{(D_q-B_q\,j\omega C_0)^2}\right), \quad (28)$$

where

$$Z_s=\sqrt{\rho G}\tanh(\gamma d) \quad (29)$$

for a single layer, or Z_s is calculated from equations analogous to Eqs. (19) and (20) for multiple layers. Even if $|Z_s/[Z_q\tanh(\gamma_qd_q/2)]|$ is as large as 0.6, the error in the motional impedance is, at most, 9%. This translates to a maximum error of 8% in the overall admittance of the loaded quartz. The result of this approximation is [from Eqs. (6)–(10) and (28)]

$$Z_m=Z_{q,m}+\frac{\mathbf{A}Z_s}{4\phi^2}, \quad (30)$$

where

$$\frac{\mathbf{A}}{4\phi^2}=\frac{\epsilon_{22}\mathbf{A}}{4C_0^2K^2\bar{c}_{66}}=\frac{\hat{k}d}{4K^2\omega C_0Z_q} \quad (31)$$

and $Z_{q,m}$ is the impedance of the motional arm for unloaded quartz. The second term in Eq. (30) is the electrical impedance, Z_e, associated with the nonpiezoelectric layers. This impedance, Z_e, is proportional to Z_s, in agreement

with Martin and Frye,[20] and, near resonance, the expression for Z_e agrees with that used by Martin and Frye. In summary, this analysis has shown that it is valid to describe lightly loaded quartz with a BVD equivalent circuit model.

1. Single layer

For any single layer, Eqs. (4) and (16) give the impedance at the quartz/layer interface

$$Z_s = \sqrt{\rho G}\tanh(\gamma d), \tag{32}$$

where γ is defined in Eq. (5). This equation agrees with that given in Martin and Frye[20] for the polymer case, and can be reduced to a thin mass layer or an infinite liquid by taking the appropriate limits. For a thin mass layer, $\gamma d \to 0$ and $\tanh(\gamma d) \to \gamma d$, so that $Z_s = j\omega\rho d = j\omega\rho_s$; for an infinite Newtonian liquid, $G = j\omega\eta$ and $\tanh(\gamma d) \to 1$, so that $Z_s = \sqrt{j\omega\rho\eta}$.

2. Two layers

a. Small $|(Z_2/Z_1)\tanh(\gamma_1 d_1)\tanh(\gamma_2 d_2)|$. If $|(Z_2/Z_1)\times\tanh(\gamma_1 d_1)\tanh(\gamma_2 d_2)|$ is much less than unity (where the subscript "2" denotes the top layer), some simplifications result, because, from Eqs. (19) and (20),

$$Z_s = \frac{jZ_2\cos(\hat{k}_1 d_1)\sin(\hat{k}_2 d_2) + jZ_1\sin(\hat{k}_1 d_1)\cos(\hat{k}_2 d_2)}{-(Z_2/Z_1)\sin(\hat{k}_1 d_1)\sin(\hat{k}_2 d_2) + \cos(\hat{k}_1 d_1)\cos(\hat{k}_2 d_2)}, \tag{33}$$

which reduces to *the sum of the impedances at the bottom of each layer*:

$$\begin{aligned} Z_s &= jZ_2\tan(\hat{k}_2 d_2) + jZ_1\tan(\hat{k}_1 d_1) \\ &= Z_2\tanh(\gamma_2 d_2) + Z_1\tanh(\gamma_1 d_1). \end{aligned} \tag{34}$$

For $|(Z_2/Z_1)\tanh(\gamma_1 d_1)\tanh(\gamma_2 d_2)| = 0.1$, the error in Eq. (34) is, at most, 11%. Note that the term $|(Z_2/Z_1)\tanh(\gamma_1 d_1)\tanh(\gamma_2 d_2)|$ represents the interaction between the two layers because it contains the ratio of the intrinsic layer impedances multiplied by the two terms representing phase shift and attenuation in each of the two layers. If one of the three components of this term is small, the interaction between the two layers can be neglected. For example, this low-interaction assumption applies to a thin (small-d), rigid (large-G) mass layer in contact with a liquid because

$$\begin{aligned} &(Z_2/Z_1)\tanh(\gamma_1 d_1)\tanh(\gamma_2 d_2) \\ &= \frac{\sqrt{j\omega\rho_2\eta_2}}{\sqrt{\rho_1 G_1}}\, j\omega\sqrt{\rho_1/G_1}\, d_1 \to 0 \end{aligned} \tag{35}$$

at small d_1/G_1. This assumption does *not* apply to a thick or rubbery polymer in contact with a liquid, however, as we show in the next section.

If a quartz resonator has a thin, rigid polymer film in contact with a liquid, it is valid to use the simple lumped-element equivalent circuit methods presented in Martin, Granstaff, and Frye.[4] These techniques may be used to extract the mass of the film and the viscosity-density product of the contacting liquid. These methods assume that the mass layer is thin and rigid enough to obey the Sauerbrey approximation, which predicts that the quartz resonant frequency is shifted lower by an amount proportional to the added mass[2] and that the amplitude of the resonance peak is unaffected by the mass loading. Another assumption inherent in the lumped-element circuit model is that the mechanical impedance of a thin mass layer is proportional to the mass of the layer and the interaction term, $|(Z_2/Z_1)\tanh(\gamma_1 d_1)\tanh(\gamma_2 d_2)|$, is small, so that the total surface mechanical impedance is the sum of the mass and liquid mechanical impedances, as described in Eq. (34). Equation (34), combined with the small-$|Z_s/[Z_q\tanh(\gamma_q d_q/2)]|$ approximation, states that the impedance in the motional arm of a BVD equivalent circuit is the sum of the quartz motional impedance, $Z_{q,m}$, and an electrical impedance, Z_e, that is proportional to the sum of the mechanical impedance of each nonpiezoelectric layer [see Eq. (30)].

The present analysis can be used to determine criteria for whether a given polymer is thin and rigid enough to use the lumped-element BVD equivalent circuit and, if not, provides an alternative data fitting method. If the BVD approximation holds, a single coated resonator in liquid is sufficient to extract the film mass and the liquid viscosity-density product simultaneously. The method for doing so is based on the fact that, while the frequency shift resulting from loading the crystal with mass and liquid depends on both the mass and the liquid, the damping (inverse of the maximum amplitude) of the quartz resonance peak $[1/(Y - j\omega C_0)]$ depends only on the liquid.[4] Observe that $j\omega C_0$ is subtracted from the admittance to eliminate the effect of the quartz on the resonance peak amplitude. Therefore, the damping gives the liquid viscosity-density product, and the frequency shift gives the mass (after correcting for the effect of the liquid on resonant frequency).

Instead of using a single crystal, an uncoated reference crystal may be placed in the same liquid as the polymer-coated sensing crystal. Clearly, the resonant frequency of the reference crystal depends only on the liquid. If the BVD approximation holds, the *difference* in resonant frequency *between the sensing and reference* crystals is proportional to the coating mass, and *independent* of the liquid. Also, the difference in the resonance peak amplitudes between the two crystals is zero because the resonance peak damping (inverse of amplitude) is equal to the resistance in the motional arm of the equivalent circuit.Since this resistance depends only on the contacting liquid, which is the same for both crystals, the maximum damping (and amplitude) of the resonance peak is identical for the two crystals. Although it is unnecessary to use a reference crystal to measure the mass of a thin layer, it is useful to understand this limiting case before proceeding to the thick-polymer case, which requires a reference crystal to extract the polymer film mass and viscoelastic properties.

b. Polymer in contact with liquid. If a quartz resonator has a thick coating, the BVD approximation does not hold, and it is difficult to extract the mass loading and the liquid viscosity-density product simultaneously from a single

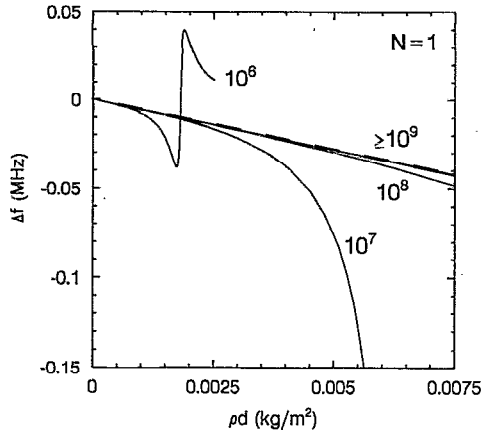

FIG. 7. Calculated effect of polymer stiffness (values in N m^{-2}) for lossless polymers in contact with water at fundamental quartz resonance. Thin or stiff polymers follow the linear Sauerbrey approximation, shown by the dashed line. (Divide ρd values by 10 to obtain g cm^{-2}, and multiply G values by 10 to obtain dyn cm^{-2}).

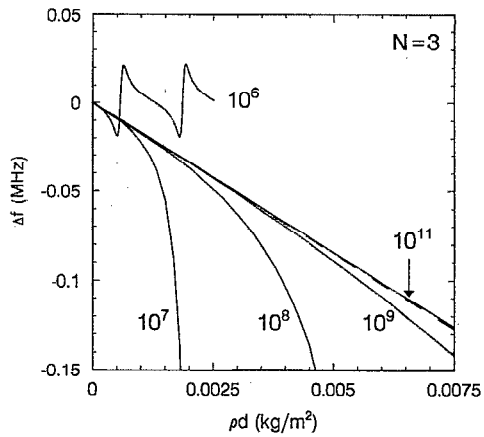

FIG. 8. Calculated effect of polymer stiffness (values in N m^{-2}) for lossless polymers in contact with water at third-harmonic quartz resonance. Thin or stiff polymers follow the linear Sauerbrey approximation (dashed line).

crystal, because the frequency shift and the resonance peak amplitude both depend nonlinearly on the liquid and the polymer film properties. Therefore, an unloaded reference crystal should be immersed in the same liquid and used to determine $\rho\eta$ separately (using the methods presented in Kanazawa and Gordon);[31] the present analysis can then be used to extract the polymer film parameters, accounting for the polymer/liquid interaction.

The breakdown of the BVD approximation occurs with thick polymers because the upper film surface no longer moves synchronously with the lower film surface. As described in Martin and Frye,[20] the upper film surface can oscillate in phase or out of phase with the lower film surface. At *polymer resonance*, a transition between these two modes occurs [at the discontinuity where $\tan(\hat{k}_1 d_1)$ changes sign]. The transition from in-phase motion to out-of-phase motion is accompanied by a sudden increase in the overall quartz resonant frequency, and a sharp *increase* in the *damping* of the resonance peak.

Figure 7 shows the polymer resonance calculated for a low-modulus, lossless polymer (the curve for $G=10^6$ N m^{-2}). Figure 7 shows Δf, the difference between the sensing crystal frequency and the constant reference crystal frequency (both immersed in the same liquid), vs the mass (ρd) of the polymer film on the sensing crystal. Note that if the thin, rigid polymer approximation held, the plot would be linear (as indicated by the dashed lines in Figs. 7 and 8). Indeed, at low ρd (thin films) or high G (stiff films), the plot follows the linear Sauerbrey approximation. However, at higher mass loadings, it deviates from linearity and demonstrates the polymer resonance described above. Recall that stiffer polymers (higher G) require a greater film mass to induce deviation from the linear Sauerbrey approximation, as shown by Eq. (35). Stiff polymers also resonate, but these resonances have larger frequency shifts and more damping of the resonance peak (proportional to G). The high-G polymer resonances are not shown because the purpose of Fig. 7 is to allow experimenters to determine whether the linear Sauerbrey approximation should hold for their particular polymers in water [or any fluid with $\rho\eta \approx 1$ (kg m^{-3}) (N s m^{-2})]. By estimating the expected ρ, d, and G, and plotting the ρd on the appropriate G curve of Fig. 7, one can determine whether the linear approximation is valid by noting how closely the plotted point matches the linear approximation. If the linear approximation holds, the analysis methods presented in Martin, Granstaff, and Frye[4] apply, and a reference crystal is unnecessary. While Fig. 7 illustrates the range of applicability of the BVD circuit methods at the fundamental quartz resonance, Fig. 8 is for the third harmonic. Observe that at the third harmonic, the deviation from linearity occurs at film masses three times lower than at the fundamental, as expected from the definition of $\hat{k}d$ [see Eq. (5)]. While Figs. 7 and 8 describe coated resonators in water, plots analogous to Figs. 7 and 8 could be constructed for a liquid with a viscosity-density product greater or less than that of water.

Another representation of the polymer resonance is a parametric plot. This array of three cross plots shows the relationships among three variables—the resonance peak damping, resonant frequency, and phase shift across the polymer film. Each of the three plots shows the relation between two of the variables; all three are plotted on the same scale and aligned for ease of comparison.

Figures 9–11 show parametric plots illustrating the effects of contacting liquid and Maxwell polymer film parameters[32] at the fundamental quartz resonance. For a Maxwell polymer film $G_f=\mu_f+j\omega\eta_f$. In these figures, the upper-left-hand plot shows the difference in the resonance peak damping between the coated (sensing) and uncoated (reference) resonators in the liquid $[\Delta 1/(Y-j\omega C_0)]$ versus the phase shift of the polymer film [the real part of $\hat{k}d$ from Eq. (5)]. Because the reference crystal is uncoated, its damping versus any polymer properties is a constant. This constant offset is subtracted from the coated resonator response in each of the parametric plots. The phase shift is a dimensionless representation of the film thickness, e.g., at

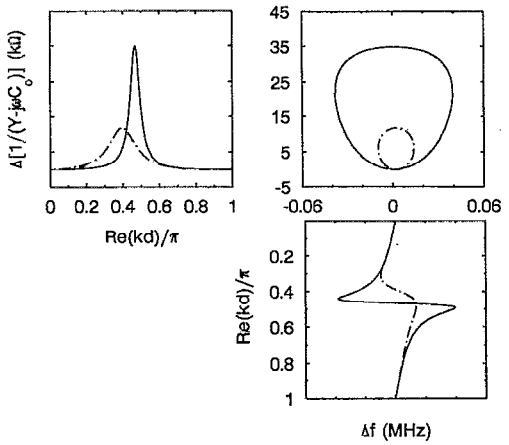

FIG. 9. Parametric plot showing resonance of a rubbery polymer ($G=10^6$ N m^{-2}) in contact with water (solid line, $\rho\eta=1$ kg m^{-3} N s m^{-2}) and a more viscous liquid (dot-dashed line, $\rho\eta=9$ kg m^{-3} N s m^{-2}). Note that the more viscous liquid reduces the polymer-induced damping.

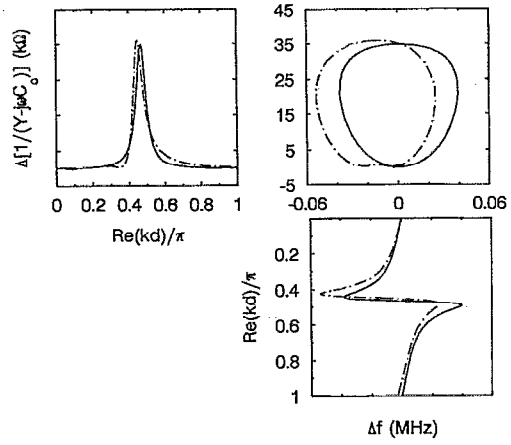

FIG. 11. Parametric plot showing effect of polymer viscosity on resonance of polymer ($\mu_f=10^6$ N m^{-2}) in contact with water [$\rho\eta=1$ (kg m^{-3}) (N s m^{-2})]. Solid line: $\eta_f=0$ N s m^{-2}; dot-dashed line: $\eta_f=3.2\times10^{-2}$ N s m^{-2}.

Re($\hat{kd}$)$=\pi$, the film thickness equals half the acoustic wavelength. Recall that if the thin, rigid film approximation held, there would be no difference in damping between the coated and uncoated resonators because they are immersed in the same liquid; therefore $\Delta(1/(Y-j\omega C_0)$ would be zero. The upper-left-hand plots show the dramatic *increase in damping that accompanies the polymer resonance* at Re($\hat{kd}$)$\approx\pi/2$, the film thickness corresponding to a quarter acoustic wavelength.

The lower-right-hand plot shows the phase shift, Re($\hat{kd}$), versus the frequency difference between the coated and uncoated resonators in liquid. At small $\hat{kd}$, where the Sauerbrey approximation holds, Δf decreases linearly with $\hat{kd}$. This lower-right-hand plot (viewed sideways) shows the frequency difference versus the dimensionless film thickness, Re($\hat{kd}$), while Figs. 7 and 8 show the frequency difference versus the film mass, ρd.

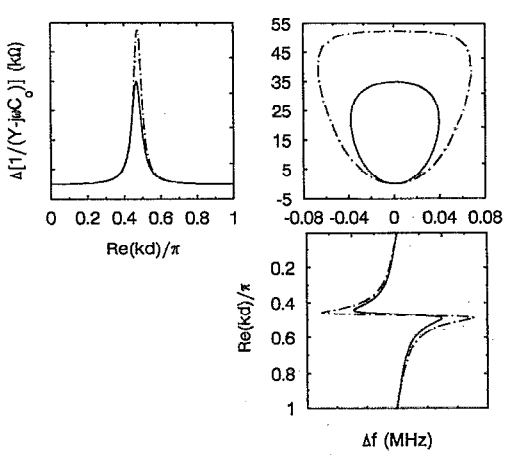

FIG. 10. Parametric plot showing effect of elasticity on resonance of a lossless polymer ($\eta_f=0$ N s m^{-2}) in contact with water [$\rho\eta=1$ (kg m^{-3}) (N s m^{-2})]. Solid line: $\mu_f=10^6$ N m^{-2}; dot-dashed line: $\mu_f=1.5\times10^6$ N m^{-2}.

The upper-right-hand plots show the damping difference versus the resonant frequency difference, which traces a loop in the clockwise direction, starting at the origin, as Re($\hat{kd}$) increases from zero to π. At the film thickness corresponding to the maximum damping, the impedance match at the quartz/film interface results in no reflection of the acoustic wave at the quartz/liquid interface. However, the plot returns to the origin at $\hat{kd}=\pi$ because the tan($\hat{kd}$) term in the polymer impedance expression is zero, making $Z_s=Z_L$ for both crystals. Physically, at $\hat{kd}=\pi$, the acoustic wave is reflected at the polymer/liquid interface; therefore the power dissipation into the liquid is minimized. If the equivalent circuit model applied and the polymer did not affect the damping of the resonance peak [$\Delta1/(Y-j\omega C_0)=0$], then the frequency change versus the uncoated resonator in liquid would be directly proportional to the film mass. These conditions would correspond to a horizontal line along the negative portion of the Δf axis (on the upper-right-hand plot). Note that at small $\hat{kd}$, the loop in the upper-right-hand $\Delta1/(Y-j\omega C_0)$-vs-Δf plot is tangent to the negative portion of the Δf axis [$\Delta1/(Y-j\omega C_0)\approx0$].

Figure 9 shows the effect of the liquid viscosity-density product on the resonator response. Because the effect of the liquid on the rubbery polymer film differs from the effect of the same liquid on the bare quartz reference crystal, *there is an interaction between the polymer and liquid*. It is not surprising, then, that the damping of the quartz resonator (versus that of an uncoated resonator in the liquid) depends on the density-viscosity product, $\rho\eta$, of the liquid. Recall that the damping of the quartz resonator versus the reference crystal is significant only near polymer resonance, where the polymer cannot be regarded as thin and rigid. As Fig. 9 shows, the maximum damping difference between the coated and uncoated resonator is inversely proportional to $\sqrt{\rho\eta}$. The reason that the damping increases, with lower $\sqrt{\rho\eta}$, is that the impedance matching between the quartz and the liquid is improving. As the

figure shows, the maximum damping occurs at approximately the quarter-wavelength film thickness. At this film thickness, perfect impedance matching occurs if the impedance of the polymer film is the geometric mean of the quartz and liquid impedances.[23] If this impedance matching condition is exactly met, there is no reflection of the acoustic wave at the quartz/polymer or the polymer/liquid interface; therefore all of the power from the oscillating quartz is radiated into the liquid (and the resonance peak is completely damped). Clearly, one should design experiments to avoid this condition, because a highly damped resonance peak is difficult to measure accurately. On the other hand, if the liquid is too viscous, both the sensing and reference crystals will have heavily damped resonance peaks, and the subtraction of two small, inaccurate numbers is likely to give inaccurate results.

Another interesting feature of Fig. 9 is that the film thickness at which maximum damping occurs decreases with liquid viscosity. Again, the impedance-matching argument explains this phenomenon. Equation (33) shows that as Z_2 (the liquid impedance) is increased, the $\tanh(\hat{k}_1 d_1)$ term must decrease to maintain the $Z_s = Z_q$ impedance-matching condition.

Figures 10 and 11 illustrate the effects of polymer film parameters for a Maxwell polymer[32] ($G_f = \mu_f + j\omega\eta_f$) in contact with water. The effect of stiffness, μ_f, is shown in Fig. 10, and the effect of viscosity, η_f, is shown in Fig. 11. As Fig. 10 shows, for stiffer polymers (larger μ_f), the loop is larger in diameter, and it stays tangent to the Δf axis for larger Δf's (and ρd's), corresponding to adherence to the Sauerbrey approximation. Also, the damping of the quartz resonance by the polymer is more severe for stiffer polymers, as seen by the larger $\Delta 1/(Y - j\omega C_0)$ maximum. Again, this increase in damping results because the polymer impedance is closer to the geometric mean of the quartz and liquid impedances.

As shown in Fig. 11, the effect of increasing the polymer viscosity, η_f, is to shift the loop toward more negative Δf's (lower resonant frequencies), even when the polymer is oscillating out of phase with the quartz. Note that, in contrast to the liquid density-viscosity product and the polymer stiffness, the polymer viscosity, η_f, affects the position of the $\Delta 1(Y - j\omega C_0)$ versus Δf loop along the Δf axis, but not the damping.

To summarize the quartz/polymer/liquid system, for low mass loading (ρd), as shown in Figs. 7 and 8, the BVD equivalent circuit method[4] is valid, and a reference crystal is unnecessary to extract the film mass and liquid properties. At larger thicknesses, the polymer and liquid impedances can no longer be added in the motional arm of a BVD equivalent circuit. If a coated sensing crystal and an uncoated reference crystal are used together in the same liquid, one can plot the sensing versus reference frequency, Δf, against the sensing versus reference damping, $\Delta 1/(Y - j\omega C_0)$. Ideally, the data should encompass a complete polymer film resonance by varying the film thickness, e.g., by electrochemically growing the polymer film. With a plot of the Δf vs $\Delta 1/(Y - j\omega C_0)$ loop, the data can be fit to determine μ_f, which affects the size of the loop (see Fig. 10) and η_f, which affects the position of the loop (see Fig. 11). The location of a data point along a given loop determines the real part of $\hat{k}d$. With the extracted $G = \mu_f + j\omega\eta_f$, d can be obtained if ρ is known *a priori*. If both ρ and d are unknown, $\sqrt{\rho d}$ can be extracted from $\hat{k}d$ using Eq. (5).

Another method for inducing a polymer resonance is to vary the temperature as in Martin and Frye.[20] Analyzing these data would be more complex because the real and imaginary parts of G depend on temperature.

IV. CONCLUSIONS

A complete one-dimensional model of a composite resonator shows that, for a *lightly loaded quartz crystal*, e.g., $|Z_s/[Z_q \tanh(\gamma_q d_q/2)] < 0.6$, *a lumped-element equivalent circuit approximation is valid*. The equivalent circuit has, in the motional arm, an impedance element, whose value is proportional to the mechanical impedance evaluated at the top quartz interface. *If the quantity representing the interaction of the two layers is small* $[|(Z_2/Z_1)\tanh(\gamma_1 d_1)\tanh(\gamma_2 d_2)| < 0.1]$, where layer 2 is above layer 1, *the mechanical impedances of these two layers may be added* to obtain the mechanical impedance at the top quartz surface. An example that meets this criterion is a thin, rigid mass layer in contact with a liquid. If either of these two conditions is not satisfied, multiple layers are still easily analyzed by the matrix methods presented here.

The viscoelastic properties (μ_f and η_f) of a polymer layer in contact with a liquid can be obtained by using an uncoated reference crystal in the same liquid as the coated sensing crystal and fitting the loop obtained by plotting the damping difference versus the frequency difference [$\Delta 1/(Y - j\omega C_0)$ vs Δf] near polymer resonance. The location of a given resonant frequency and resonance peak amplitude along this loop determines the film thickness or density.

Many applications, such as chemical sensors and advanced battery development, can benefit from the ability to extract the thickness and viscoelastic properties of polymer films in liquids. We have presented methods for analyzing admittance versus frequency data taken from a polymer-coated quartz resonator immersed in a liquid. We have also presented general methods that apply to a piezoelectric resonator having any number of arbitrarily thick nonpiezoelectric layers.

ACKNOWLEDGMENTS

The authors gratefully acknowledge Professor R. S. Savinell (Case Western Reserve University) for suggesting the idea of a criterion for determining the applicability of the BVD equivalent circuit, and D. B. Adolf and G. C. Frye (both of Sandia) for helpful discussions. This work was performed at Sandia National Laboratories, which is operated for the U.S. Department of Energy under Contract No. DE-AC04-76DP00789.

NOMENCLATURE

a,b	impedances involved in $A_q - D_q$ [Eqs. (7a) and (7b)] ($\mathrm{kg\,s^{-1}\,m^{-2}}$)
A',B'	2×2 matrix entries for obtaining the outputs
C',D'	from the inputs
A,B	2×2 matrix entries for obtaining the inputs from
C,D	the outputs [Eqs. (3a)–(3d)]
A_n,B_n	2×2 matrix entries for obtaining the inputs
C_n,D_n	from the outputs for the nth layer
A_q,B_q	2×2 matrix entries for the quartz piezoelectric
C_q,D_q	layer [Eqs. (6a)–(6d)]
$\mathbf{A}$	active electrode area ($\mathrm{m^2}$)
C_0	static capacitance of AT-cut quartz resonator ($4.029\times10^{-12}\ \mathrm{A^2\,s^4\,kg^{-1}\,m^{-2}}$)
C_1,L_1	electrical motional impedance elements associated
R_1	with uncoated resonator
$\bar{c}_{66}$	piezoelectrically stiffened elastic constant for lossless quartz ($2.947\times10^{10}\ \mathrm{N\,m^{-2}}$)
$\bar{\bar{c}}_{66}$	piezoelectrically stiffened elastic constant for lossy quartz ($\mathrm{N\,m^{-2}}$)
d	layer thickness (m)
d_q	quartz thickness (m)
d_n	thickness of nth layer (m)
e_{26}	piezoelectric stress constant for quartz ($9.53\times10^3\ \mathrm{A\,s\,m^{-2}}$)
f	excitation frequency (Hz)
Δf	resonant frequency difference between sensing and reference crystals (Hz)
G,G_f	complex shear modulus of film ($\mathrm{N\,m^{-2}}$)
h	piezoelectric term [Eq. (10)]
I	current (representing acoustical particle velocity)
I_i	input current
I_n	acoustical current at top of nth layer ($\mathrm{m\,s^{-1}}$)
I_o	output current
I_q	acoustical current at top of quartz ($\mathrm{m\,s^{-1}}$)
j	$(-1)^{1/2}$
$\hat{k}$	complex shear propagation constant ($\mathrm{m^{-1}}$)
$\hat{k}_n$	complex shear propagation constant for nth layer ($\mathrm{m^{-1}}$)
$\hat{k}_q$	complex shear propagation constant for quartz ($\mathrm{m^{-1}}$)
K^2	electromechanical coupling factor for lossy quartz [Eq. (25a)]
K_0^2	electromechanical coupling factor for lossless quartz [Eq. (25b)] (7.74×10^{-3})
N	harmonic number or number of layers on quartz
Q_n	complex parameter for nth layer [Eq. (13)]
V	voltage (representing acoustical shear stress)
V_i	input voltage
V_n	acoustical voltage at top of nth layer
V_o	output voltage
V_q	acoustical voltage at top of quartz ($\mathrm{kg\,m^{-1}\,s^{-2}}$)
Y	electrical admittance (inverse of impedance) of composite resonator ($\mathrm{A^2\,s^3\,kg^{-1}\,m^{-2}}$)
Y_m	electrical motional admittance ($\mathrm{A^2\,s^3\,kg^{-1}\,m^{-2}}$)
Z	characteristic impedance of a transmission line
Z_e	complex electrical impedance representing the load on the quartz ($\mathrm{kg\,m^2\,s^{-3}\,A^{-2}}$)
Z_L	load impedance terminating a transmission line
Z_m	electrical motional impedance ($\mathrm{kg\,m^2\,s^{-3}\,A^{-2}}$)
Z_n	impedance V_n/I_n
Z_q	quartz characteristic impedance ($\mathrm{kg\,s^{-1}\,m^{-2}}$)
$Z_{q,m}$	quartz motional impedance ($\mathrm{kg\,m^2\,s^{-3}\,A^{-2}}$)
Z_s	surface (shear) mechanical impedance ($\mathrm{kg\,s^{-1}\,m^{-2}}$)
γ,γ_n	shear wave propagation constant for nth layer ($\mathrm{m^{-1}}$)
ϵ_{22}	quartz permittivity ($3.982\times10^{-11}\ \mathrm{A^2\,s^4\,kg^{-1}m^{-3}}$)
η,η_f	film viscosity ($\mathrm{N\,s\,m^{-2}}$)
η_q	effective viscosity of quartz ($3.5\times10^{-4}\ \mathrm{kg\,m^{-1}\,s^{-1}}$)
μ_f	film shear stiffness ($\mathrm{N\,m^{-2}}$)
μ_q	quartz shear stiffness ($\mathrm{N\,m^{-2}}$)
ξ	loss parameter for quartz [Eq. (25d)]
ρ	mass density of film ($\mathrm{kg\,m^{-3}}$)
ρ_q	quartz mass density ($2.651\times10^3\ \mathrm{kg\,m^{-3}}$)
ρ_s	film areal mass density ($\mathrm{kg\,m^{-2}}$)
ϕ	transformer turns ratio ($\mathrm{A\,s\,m^{-1}}$)
ω	angular frequency ($2\pi f$) ($\mathrm{s^{-1}}$)
ω_s	angular series resonant frequency ($\mathrm{s^{-1}}$)

[1] E. Benes, J. Appl. Phys. **56**, 608 (1984).
[2] G. Sauerbrey, Z. Phys. **155**, 206 (1959).
[3] K. H. Behrndt, J. Vac. Sci. Technol. **8**, 622 (1971).
[4] S. J. Martin, V. E. Granstaff, and G. C. Frye, Anal. Chem. **63**, 2272 (1991).
[5] K. K. Kanazawa and S. K. Doss, Plat. Surf. Fin. 52 (July, 1987).
[6] A. R. Hillman, D. C. Loveday, M. J. Swann, S. Bruckenstein, and P. C. Wilde, *Biosensors and Chemical Sensors*, American Chemical Society Symposium Series (American Chemical Society, Washington, DC, 1992), Chap. 12, p. 150.
[7] M. R. Deakin and D. A. Buttry, Anal. Chem. **61**, 1147A (1989).
[8] D. A. Buttry, Electroanal. Chem. **17**, 1 (1990).
[9] R. Schumacher, Angew. Chem., Int. Ed. Engl. **29**, 329 (1990).
[10] H. Wiese and K. G. Weil, Ber. Bunsenges. Phys. Chem. **91**, 619 (1987).
[11] M. Benje, M. Eiermann, U. Pittermann, and K. G. Weil, Ber. Bunsenges. Phys. Chem. **90**, 435 (1986).
[12] M. Seo, I. Sawamura, and N. Sata, Extended Abstracts, Electrochemical Society Fall Meeting, Seattle, WA, 1990 (unpublished), Abstract No. 187, p. 272.
[13] H. Hager, L. Sigalla, T. Nellikkattil, and N. Olson, Extended Abstracts, Electrochemical Society Fall Meeting, Chicago, IL, 1988 (unpublished), Abstract No. 744, p. 1065.
[14] J. Desilvestro, W. Scheifele, and O. Haas, J. Electrochem. Soc. **139**, 2727 (1992).
[15] H.-K. Park, K. Podolske, Z. Munshi, W. H. Smyrl, and B. B. Owens, J. Electrochem. Soc. **138**, 627 (1991).
[16] G. T. Cheek and W. E. O'Grady, *Proceedings of the Electrochemical Society, Proceedings of the Symposium on Applied Surface Analytical Methods* (The Electrochemical Society, Pennington, NJ, 1990), Vol. 91-7, p. 248.
[17] A. R. Hillman, D. C. Loveday, M. J. Swann, S. Bruckenstein, and C. P. Wilde, J. Chem. Soc. Faraday Trans. **87**, 2047 (1991).
[18] P. J. Cumpson and M. P. Seah, Meas. Sci. Technol. **1**, 544 (1990).
[19] M. D. Ward and E. J. Delawski, Anal. Chem. **63**, 886 (1991).
[20] S. J. Martin and G. C. Frye, 1991 Ultrasonics Symposium Proceedings (unpublished), p. 393.
[21] C. S. Lu and O. Lewis, J. Appl. Phys. **43**, 4385 (1972).
[22] C. Lu, J. Vac. Sci. Technol. **12**, 578 (1975).
[23] S. Ramo, J. R. Whinnery, and T. Van Duzer, *Fields and Waves in Communication Electronics* (Wiley, New York, 1965).
[24] A. Ballato, H. L. Bertoni, and T. Tamir, IEEE Trans. Microwave Theory Tech. **MTT-22**, 14 (1974).

[25] J. F. Rosenbaum, *Bulk Acoustic Wave Theory and Devices* (Artech House, Boston, 1988).
[26] S. J. Martin, G. C. Frye, A. J. Ricco, and S. D. Senturia, Anal. Chem. **65**, 2910 (1993).
[27] C. E. Reed, K. K. Kanazawa, and J. H. Kaufman, J. Appl. Phys. **68**, 1993 (1990).
[28] D. K. Edwards, Int. J. Heat Mass Transfer. **25**, 815 (1982).
[29] R. J. Smith, *Circuits, Devices, and Systems*, 3rd ed. (Wiley, New York, 1976), Chap. 8.
[30] H. B. Dwight, *Tables of Integrals and Other Mathematical Data* (Macmillan, New York, 1961).
[31] K. K. Kanazawa and J. G. Gordon, II, Anal. Chem. **57**, 1770 (1985).
[32] J. D. Ferry, *Viscoelastic Properties of Polymers*, 3rd ed. (Wiley, New York, 1980).